JOURNAL OF CATALYSIS 142, 392–405 (1993)

NiO Reducibilities: Structural and Catalytic Properties of Their Pure and Potassium-Doped Reduced Forms

FRANCISCO MEDINA,[1] PILAR SALAGRE,[1] JOSÉ L. G. FIERRO,[2] AND JESÚS E. SUEIRAS[1]

[1]*Dpt. de Química, Facultat de Química de Tarragona, Universitat de Barcelona, Pl. Imperial Tarraco 1, 43005 Tarragona, Spain; and* [2]*Instituto de Catálisis y Petroleoquímica, C.S.I.C., Campus UAM, Cantoblanco, 28049 Madrid, Spain*

Received October 9, 1992; revised January 29, 1993

The study of the activation energies of reduction of stoichiometric and nonstoichiometric potassium-free and potassium-doped NiO was carried out by means of temperature-programmed reduction experiments, using two compared theoretical methods. Nonstoichiometric NiO shows the lower initial activation energy of reduction, whereas stoichiometric NiO shows a higher initial activation energy for starting the autocatalytic nucleation. Studies of the chemical preparation, BET surface areas, X-ray diffraction, X-ray photoelectron spectra, scanning electron microscopy, and measurements of catalytic activities of the nickel samples for the catalytic hydrogenation of 1,6-hexanedinitrile, in a continuous process at 1 atm pressure and 443 K, in the absence of ammonia, were also carried out. Surface areas dcrease when NiO reduction temperature increase. XRD, XPS, TPR, and SEM measurements detect NiO incipiently reduced between 463 and 498 K, a NiO reducibility inhibitor character for potassium, and 99.9% reduction above 573 K for all NiO forms. 100% selectivities with respect to 6-aminohexanenitrile may be obtained at 60% conversions for catalysts with potassium contents of 10.5×10^{-4} g K_2O/g Ni on reduced nonstoichiometric NiO. A mechanism for the continuous process is proposed.

INTRODUCTION

The selective hydrogenation of aliphatic nitriles and dinitriles to primary amines is a classical catalyzed organic reaction of industrial interest in the manufacture of nylon-6,6. This reaction is usually carried out in the liquid phase in batch reactors at elevated hydrogen pressures (270–600 bar), where the choice of catalyst is an important factor in obtaining selectivity for primary amines. Catalysts based on Co, Ni, Ru, Cu, Rh, Pd, Pt, Mn, and Fe have been reported (*1–6*). Assays of Raney nickel and Raney cobalt catalysts have also been reported in numerous publications (*7–17*). Generally, excess of ammonia is found essential to suppress secondary and tertiary amine formation in batch systems, presumably due to the formation of an imine intermediate (*18*). Here, it is important to note the lack of reported catalyst characterization results (19, 20), since most of the literature available is composed of patents. Although nickel oxide has become an important precursor for nickel catalysts, little has been published (*21*) concerning the study of the activation energy values for the reduction of stoichiometric green NiO compared to those of nonstoichiometric black NiO. For this purpose, temperature programmed reduction (TPR) is a highly sensitive technique, which does not depend on any specific property of the catalyst, other than that the species under study be in a reducible condition (*22*). Thus, we report here the study of the activation energies of NiO reduction from TPR data, always bearing in mind that TPR experimental conditions may not be the same as the reduction conditions in the reactor. Also, a potassium-doped nonstoichiometric NiO was included in the study in order to quantify the reduction inhibiting effect of potassium on NiO. To perform this study the approaches of Coats and Redfern (*23*) and of Ozawa *et al.* (*24*) were followed according

0021-9517/93 $5.00

to the theory of nonisothermal reductions of a (solid + gas) reactant system.

Beside the TPR measurements and activation energy calculations, further surface structural characterizations of the oxide precursors and the reduced nickel catalysts were carried out in this study, using BET, XRD, XPS, and FE-SEM techniques, in order to explain their different behaviour as catalysts for the hydrogenation of 1,6-hexanedinitrile, under flow reaction conditions and 1 atm pressure, where some of them showed remarkable primary amine selectivities in the absence of ammonia.

EXPERIMENTAL

Catalyst Preparation

The black nonstoichiometric NiO precursor was prepared by air calcination of nickel nitrate hexahydrate at 673 K. Potassium-doped nickel precursors were prepared by impregnation of the previously calcined nickel nitrate hexahydrate with the relevant doping amounts of potassium nitrate aqueous solutions, as shown in Table 1, followed by drying at 393 K for 5 h. The green stoichiometric NiO precursor was prepared by further heating of the black nonstoichiometric NiO at 1173 K for 4 h in the oven. All samples were reduced with hydrogen/argon for 20 h, with a 1/20 volume ratio, an initial space velocity of 360 h^{-1} (with respect to the active gas), and temperatures shown in Table 1. These preparations will be designated hereafter as catalysts 1–5, 6–11, and 12–21 when arising from the green, black, and potassium-doped black NiO, respectively.

All reagents were reagent-grade (from Aldrich Co.), and pure gases were previously dried and deoxygenated.

Air-Free Sampling

The catalysts were always handled under air-free conditions after the reduction step. The catalysts were transferred in isooctane and under hydrogen atmosphere at room temperature. The isooctane surface-impregnated samples were further isolated from the air with sticky tape and mounted for XRD monitoring. Alternatively, they were vacuum pumped for the other characterization techniques used. The catalytic activity measurements were carried out *in situ* in the same reactor after reduction; gas purges, positive gas pressures, and Schlenk techniques were used when necessary.

Temperature-Programmed Reduction (TPR)

Temperature-programmed reductions were carried out in a Perkin–Elmer TGA 7 microbalance with an accuracy of 1 μg, equipped with a 273–1273 K programmable temperature furnace. Samples weighing 25 mg were first heated at 4 K min^{-1} to 673 K in a stream of He (80 $cm^3 min^{-1}$) for moisture release. After cooling to room temperature under helium, they were heated again in a 5 vol% H_2/Ar flow (80 cm^3 min^{-1}) to reduction temperatures between 443 and 623 K. The weight change in the samples is a measure of the oxygen released by the solid as water.

BET Surface Areas

BET surface areas were calculated from the nitrogen adsorption isotherms at 77 K using a Micromeritics ASAP 2000 surface analyzer and a value of 0.164 nm^2 for the cross-section of the nitrogen molecule.

X-Ray Diffraction (XRD)

Powder X-ray diffraction patterns of the catalysts were obtained with a Philips PW 1010 diffractometer using nickel-filtered Cu$K\alpha$ radiation. Samples were dusted on double-sided sticky tape and mounted on glass microscope slides. The patterns were recorded over a range of 2θ angles from 5° to 85° and compared with the X-ray powder files to confirm phase identities.

X-Ray Photoelectron Spectroscopy (XPS)

X-ray photoelectron spectra were recorded on a Leybold LHS 10 spectrome-

TABLE 1

XRD and XPS Characterization and Catalytic Properties[a] of Several Potassium-Free and Potassium-Doped Nickel Catalysts vs Reduction Temperatures

Catalyst	1	2	3	4	5	6	7	8	9	10	11	12	13	14	15	16	17	18	19	20	21
g K_2O/g Ni ($\times 10^{-4}$)	—	—	—	—	—	—	—	—	—	—	—	7	7	7	7	7	10.5	10.5	10.5	10.5	10.5
Reduction temp. (K)	573	598	623	648	673	443	463	473	498	573	673	473	498	573	623	673	498	573	623	673	723
Cryst. phases (XRD)	NiO	NiO	Ni	Ni	Ni	NiO	NiO	NiO	Ni	Ni	Ni	NiO	NiO + Ni	Ni	Ni	Ni	NiO + Ni	Ni	Ni	Ni	Ni
Binding Energy (XPS) from Ni $2p_{3/2}$ level (eV)	855.8	855.6	854.6	854.5	854.4	855.8	855.7	855.6	854.5	854.4	854.2	855.8	855.0	854.4	854.3	854.2	855.6	854.8	854.4	854.3	854.2
Conversion (%)	0	10	50	30	5	0	78	80	100	100	33	10	47	92	65	50	12	35	50	60	15
Selectivity (%) to:																					
monoamine	—	90	50	80	93	—	63	50	0	15	100	100	80	20	43	80	100	100	100	100	100
diamine	—	0	5	4	0	—	27	30	30	20	0	0	0	23	24	15	0	0	0	0	0
others	—	10	45	16	7	—	10	20	70	65	0	0	20	57	33	5	0	0	0	0	0

Note. Samples 1–5 derive from stoichiometric NiO, samples 6–11 from non-stoichiometric NiO.

[a] Monoamine = 6-aminohexanenitrile; diamine = 1,6-hexanediamine; others = azacycloheptane, mainly. Reaction conditions: 1,6-hexane dinitrile hydrogenation at 443 K, 1 atm pressure, and a space velocity of 1500 h^{-1}.

ter provided with a Mg$K\alpha$ X-ray radiation source and a hemispherical energy analyzer. Powdered samples were pressed into small stainless steel cylinders and mounted on a standard sample probe, placed in a preevacuation chamber evacuable to ca. 10^{-5} Torr, before they were moved into the main vacuum chamber. The residual pressure in the turbo-pumped analysis chamber was kept below 7×10^{-9} Torr during data collection. Each spectral region was signal-averaged for a given number of scans to obtain good signal-to-noise ratios. Although surface charging was observed on all the samples, accurate binding energies (BE) were determined by charge referencing with the C 1*s* line at 284.6 eV. Peak areas were computed by a program which assumed Gaussian lines and flat background subtraction.

Scanning Electron Microscopy (FE-SEM and SEM)

Scanning electron micrographs were obtained in a Leica Stereoscan 360 FE microscope equipped with the Field Emission system, operating at an acceleration voltage of 5 kV, a working distance of 5 mm, and magnification values of 50.000×. Scanning electron micrographs were also taken at 20 kV voltages.

Catalytic Activity Determination

In a typical experiment, the catalyst (1 g) was placed in a fixed-bed flow reactor for hydrogenation of adiponitrile vapor at 443 K and 1 atm pressure, with a molar adiponitrile/hydrogen ratio of 1/300 (high H_2 flow rates are used to favour 1,6-hexanedinitrile transport at 443 K) at a space velocity of 1500 h^{-1}. Catalysts did not show diffusion restrictions. Reaction products were analyzed by means of an on-line gas-chromatograph HP 5840A equipped with a 25-m phenylmethylsilicone capillary column, using a 343–573 K oven temperature program.

Conversion and selectivity are defined by the following equations: Conversion (%) = [moles of 1,6-hexanedinitrile consumed] × 100/[moles of 1,6-hexanedinitrile charged]. Selectivity (%) = [moles of a particular product of reaction] × 100/[moles of 1,6-hexanedinitrile consumed].

RESULTS AND DISCUSSION

Temperature Programmed Reduction

To study the reducibility of NiO and the calculation of the activation energy values for the non-isothermal reductions of the (solid + excess gas) systems involved from the TPR data, the methods of Coats and Redfern (*23*) and of Ozawa *et al.* (*24*) were applied.

Coats and Redfern (*23*) derive the following integrated equations, after rearranging the Arrhenius equation and the rate of reaction with temperature function of time, for the reaction orders $n = 0$,

$$\log\left[\frac{\alpha}{T^2}\right] = \log\frac{AR}{\beta E}\left[1 - \frac{2RT}{E}\right] - \frac{E}{2.3RT}, \quad (1)$$

and $n = 1$,

$$\log\left[-\log\frac{(1-\alpha)}{T^2}\right] = \log\frac{AR}{\beta E}\left[1 - \frac{2RT}{E}\right] - \frac{E}{2.3RT} \quad (2)$$

where α = reduction degree at time t, T = temperature (K), A = Arrhenius frequency factor, R = molar gas constant, β = linear heating rate, and E = activation energy.

Straight lines from plots of $\log(\alpha/T^2)$ vs. $1/T$, for $n = 0$, and $\log[-\log((1-\alpha)/T^2)]$ vs. $1/T$, for $n = 1$, were obtained with correlation coefficients >0.99. From the slopes, the activation energies were calculated for $\beta = 0.1$, 0.2, 0.5, and 0.8 K min^{-1}.

On the other hand, Ozawa *et al.* (*24*) derive another equation, independent of the reaction order, based on the measure of temperatures for each reduction degree, α, and different β values:

TABLE 2

Activation Energies of Reduction of Nonstoichiometric NiO for $\beta = 0.2$

α	E (kJ/mol) by method of Coats and Redfern		E (kJ/mol) by method of Ozawa *et al.*
	$n = 0$	$n = 1$	
0.2	242	4.5	228
0.4	127	7.9	175
0.6	93	11.3	150
0.75	69	16.5	144

$$\frac{d\log\beta}{d(1/T)} = (0.457/R) \cdot E. \qquad (3)$$

The plots of log β vs. $1/T$ at constant α yield straight lines, where the activation energies were obtained from the slopes at different α values. The correlation coefficients were >0.99 and the activation energies obtained by the two methods were compared for the different nickel oxides, as shown in tables below.

Table 2 shows the activation energies of reduction (kJ/mol) of nonstoichiometric black nickel oxide obtained independently of the reaction order (Ozawa *et al.*'s method), and for $n = 0$ and 1 (Coats and Redfern's method), for $\beta = 0.2$, bearing in mind that a stoichiometric excess of hydrogen gas was passed through the solid oxide and that water was continuously removed from the surface by the stream of gas, as described in the Experimental section. The decreasing activation energies with the increasing reduction degrees obtained by the Ozawa *et al.* and Coats–Redfern (only for $n = 0$) methods and the typical sigmoidal or S-shaped α against time reduction isotherms are in agreement with the nucleation model of nickel oxide reduction, where an autocatalytic process of metallic nucleus growth takes place on the surface of nickel oxide with increased degree of reduction (*25*). In this respect, we obtained pictures by field emission scanning electron microscopy, such as that in Fig. 5, which show the presence of reduced nickel particles on the surface of the nonstoichiometric nickel oxide octahedra, clearly supporting the nucleation model of reduction. Consequently, a reaction order of $n = 1$ was discarded since an incoherent trend as a function of the degree of reduction was obtained, as depicted in Table 2.

The activation energies obtained by the method of Ozawa *et al.* are somewhat higher than those obtained by the Coats–Redfern method for $\alpha > 0.3$. We should remark here that the experimental conditions fixed on a thermobalance may not match those of the reaction process, i.e., weights of the samples, shape of container (thermobalance basket against a tubular reactor), efficiency of water removal, temperature gradients, etc., in which the real activation energies, in the reactor, are higher than those obtained in the thermobalance. Consequently, we should consider more the relative character of the activation energies obtained by the two methods, rather than their absolute values.

Tables 3 and 4 show the activation ener-

TABLE 3

Activation Energies of Reduction of Stoichiometric NiO

β	α	E (kJ/mol) by method of Coats and Redfern ($n = 0$)	E (kJ/mol) by method of Ozawa *et al.*
0.1	0.2	516	
0.2	0.2	339	163
0.5	0.2	316	
0.1	0.4	268	
0.2	0.4	169	140
0.5	0.4	133	
0.1	0.6	167	
0.2	0.6	103	116
0.5	0.6	64	
0.1	0.75	95	
0.2	0.75	69	100
0.5	0.75	42	

TABLE 4

Activation Energies of Reduction of Nonstoichiometric NiO

β	α	E (kJ/mole) by method of Coats and Redfern (n = 0)	E (kJ/mole) by method of Ozawa *et al.*
0.1	0.2	460	
0.2	0.2	242	228
0.5	0.2	202	
0.8	0.2	91	
0.1	0.4	164	
0.2	0.4	127	175
0.5	0.4	95	
0.8	0.4	84	
0.1	0.6	116	
0.2	0.6	93	150
0.5	0.6	82	
0.8	0.6	43	
0.1	0.75	77	
0.2	0.75	69	144
0.5	0.75	62	
0.8	0.75	22	

gies of reduction of the stoichiometric and nonstoichiometric NiO respectively, obtained for different β values from the Coats–Redfern (for n = 0) and Ozawa *et al.* methods. A decrease of the activation energy values with increasing α is always obtained by the two methods, values obtained for the nonstoichiometric NiO by the Coats–Redfern method (Table 4) being smaller than those obtained for the stoichiometric NiO (Table 3). This result is in agreement with our experimental observation, since nonstoichiometric NiO starts and finishes its reduction about 100 K before the stoichiometric NiO (*20*, *26*, *27*). Regarding this, Fig. 1 shows a thermogram that plots not only the different initial and final reduction times (at a scanning rate of 0.2 K/min), but also the final weight change of 1.5% between both the stoichiometric and nonstoichiometric NiO that corresponds to the nonstoichiometric formula $NiO_{1.095}$. Figure 2 also supports the above results. However, the larger activation energies of reduction obtained for the nonstoichiometric NiO (Table 4) when compared with those of the stoichiometric NiO (Table 3) calculated by the Ozawa *et al.* method make no sense from our experimental evidence. Thus, the Coats–Redfern method fitted better to our experimental results in this work.

Table 5 depicts the activation energies of reduction obtained for two different potassium-doped nonstoichiometric NiO samples by the Coats–Redfern method, for β = 0.2, which is the β value closer to our reactor experimental conditions. The obtained values decrease with increased degree of reduction degree for both potassium contents, and activation energies show larger values with increased potassium content (see also Table 2, for β = 0.2). These results are in agreement with those of Fig. 2 and others previously reported (*28*, *29*), as it is found that potassium inhibits the reducibility of NiO.

Figure 3 plots the activation energy values against degree of reduction, α, for β = 0.2, and all the samples studied. Even though this information is contained in Tables 2–5, however, a new feature may be extracted from Fig. 3. Thus, the activation energies of NiO, whether it is stoichiometric or not, potassium-doped or not, follow exponential curves that converge to about the same value for reduction degrees close to 1, whereas the activation energy of the nonstoichiometric NiO may be about 60% that of the stoichiometric NiO, reaching the potassium-doped nonstoichiometric NiO intermediate values, for reduction degrees close to zero. Those convergent exponential curves are also in agreement with the reduction autocatalytic model of nickel nucleation from the starting oxide. The activation energy is always higher at the beginning of reduction until nucleation starts, for any NiO. Also, the defective nonstoichiometric NiO starts reduction at a lower temperature than the stoichiometric NiO, showing a smaller initial activation energy of reduction than the latter.

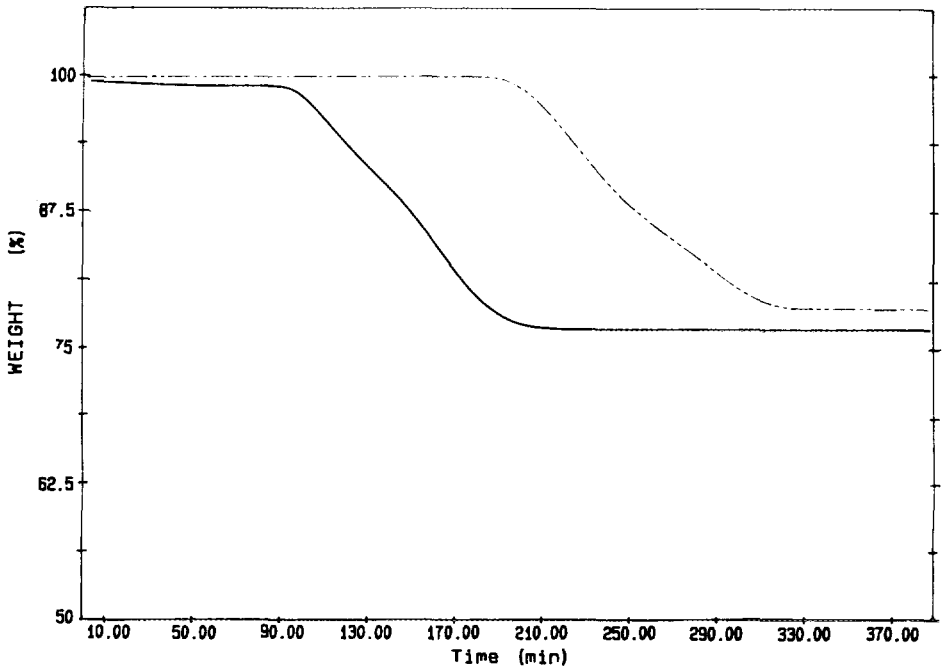

FIG. 1. Plot of weight change (%) vs time for the temperature-programmed reduction of stoichiometric NiO (dotted line) and nonstoichiometric NiO (continuous line): initial temperature 443 K; rate of heating 0.5 K min^{-1}.

BET Surface Areas

The BET surface areas of the catalysts are plotted against temperature of reduction of their precursors in Fig. 4. As expected, the surface areas are rather low. The most important features to be noted are the linear decrease in surface area of metallic nickel with increasing reduction temperatures in the range of temperatures tested, above 498 K. Such a decrease is due to a progressive increase of reduced particle sizes with temperature. Only if the nonstoichiometric NiO phase is also present do the areas rise considerably, due to their adding different phase areas; i.e., unreduced K-doped nonstoichiometric NiO exhibited 12 m^2g^{-1}, and highly reduced K-doped nonstoichiometric NiO < 1.5 m^2g^{-1}. Then, any mixture of phases shows intermediate values. The surface area differences between the extrapolated straight line and the experimental curves (Fig. 4) fit the surface area increment due to the unreduced K-doped NiO phase contribution below 623 K. This plot may also be used for estimation of the reduction degrees of potassium-doped nickel catalysts from measured BET areas. The stoichiometric NiO shows very little change of the surface area between the unreduced oxide (1.75 m^2/g) and its reduced form (1.0 m^2/g), as shown in Fig. 4, due to high sintering present in the original unreduced stoichiometric NiO. Table 6 shows the large difference between the particle sizes of the unreduced oxides, which agrees with their different sintering features, as shown below.

X-Ray Diffraction

Powder diffraction patterns of the reduced catalysts showed diffraction peaks at 2θ angles and relative intensities which can be indexed to the NiO and Ni phases. The 2θ angles and the relative intensities (in parentheses) are summarized as follows: 44.51

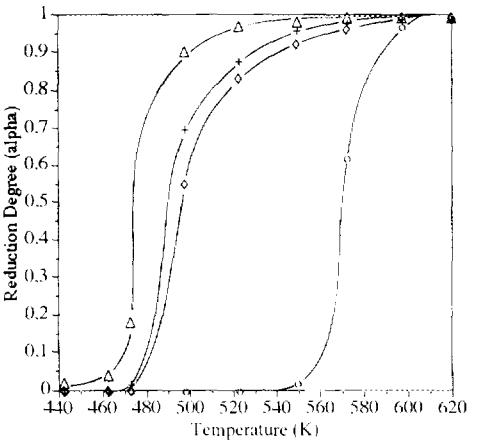

FIG. 2. Plot of reduction degree α vs temperature for nonstoichiometric NiO (Δ), potassium-doped (7×10^{-4} g K_2O/g Ni) nonstoichiometric NiO (+), potassium-doped (10.5×10^{-4} g K_2O/g Ni) nonstoichiometric NiO (◇), and stoichiometric NiO (○).

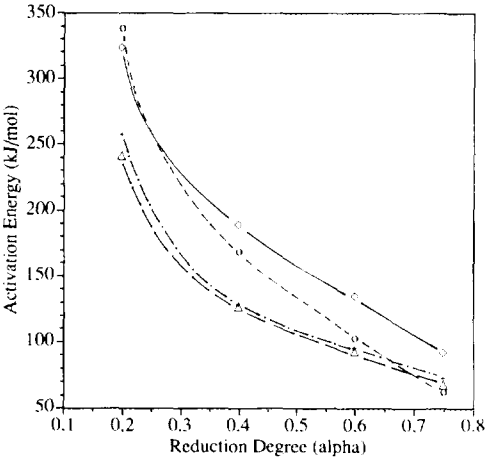

FIG. 3. Plot of activation energies, calculated by the method of Coats and Redfern ($n = 0$, and $\beta = 0.2$), vs reduction degrees α, for nonstoichiometric NiO (Δ), potassium-doped (7×10^{-4} g K_2O/g Ni) nonstoichiometric NiO (+), potassium-doped (10.5×10^{-4} g K_2O/g Ni) nonstoichiometric NiO (◇), and stoichiometric NiO (○).

(100), 51.85 (42), 76.36 (21), for the Ni phase; 37.29 (91), 43.30 (100), 62.91 (57), 75.43 (16), for the NiO phase. Potassium phases were undetectable owing to their very low concentrations.

The crystalline phases in Table 1 were obtained at different temperatures of reduction of stoichiometric NiO and potassium-free and potassium-doped nonstoichiometric NiO. The stoichiometric NiO shows the phase change, by XRD, at reduction temperatures higher than 623 K (Table 1). The incipiently reduced stoichiometric NiO is also detected when reduced at 598 K, since it starts to be catalytically active at this temperature (Table 1), although the reduced nickel phase is not detected by the XRD technique, presumably because of the presence of crystallite sizes smaller than 40 Å.

TABLE 5

Activation Energies of Reduction of Potassium-Doped Nonstoichiometric NiO, obtained by Method of Coats and Redfern for $n = 0$ and $\beta = 0.2$

α	E(kJ/mole) for catalysts 12–16	E (kJ/mole) for catalysts 17–21
0.2	258	324
0.4	129	190
0.6	96	135
0.75	73	93

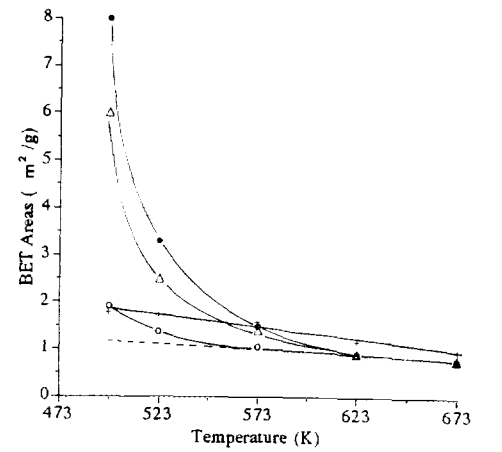

FIG. 4. Plot of BET areas vs reduction temperature for nonstoichiometric NiO (○), potassium-doped (7×10^{-4} g K_2O/g Ni) nonstoichiometric NiO (Δ), potassium-doped (10.5×10^{-4} g K_2O/g Ni) nonstoichiometric NiO (●), and stoichiometric NiO (+).

TABLE 6

NiO Crystallite Sizes (Å) from Two Methods

	B.E.T.	Scherrer
Stoichiometric NiO	4283	412
Nonstoichiometric NiO	647	305

generally undetectable by conventional spectrometers.

Reduction of nonstoichiometric NiO (samples 6–11) yields metallic nickel, at reduction temperatures of 473–498 K, with the simultaneous disappearance of the NiO phase, this being complete at 498 K. Also, previous particle size calculations using the Scherrer equation indicate the presence of larger particle sizes with increasing temperatures of reduction of NiO precursors, in line with the sharp decrease of BET areas in that range of reduction temperatures. While the NiO–Ni phase change takes place between 473 and 523 K for the potassium-free nickel catalysts, this phase change takes place at higher temperatures for the potassium-doped catalysts, which is evidence for the probable presence of a superficial potassium–nickel-oxide phase which is difficult to reduce. These results agree with those obtained from the temperature-programmed reductions.

The fact that pure NiO samples were totally inactive for nitrile hydrogenation in the experimental conditions used in this study points out that only reduced nickel is the active phase involved in the reaction. Catalysts 7 and 8, which do not show diffraction lines of metallic nickel, are nevertheless catalytically active (Table 1). This behavior may reasonably be explained assuming the formation of some kind of incipiently reduced surface nickel, probably with very small crystallite sizes, below the detection limits of current powder X-ray diffractometers. In order to confirm this interpretation, XPS and SEM surface characterizations of several catalysts concerned have been carried out.

The XRD data from Table 1 show the presence of reduced potassium-doped nonstoichiometric NiO at temperatures higher than 523 K. This reduction has been complete for potassium-free samples at lower temperatures, under the same experimental conditions. Reduction temperatures needed rise with potassium content. Consequently, potassium inhibits the NiO reducibility under hydrogen. In line with the incipient reduction of the potassium-free catalysts with very small crystalline sizes, reduced between 463 and 473 K, the same situation is obtained for the potassium-doped catalysts at higher reduction temperatures between 473 and 498 K, depending on potassium contents, as tested in this work.

NiO Crystallite Sizes

The only difference between the diffraction patterns of both the stoichiometric and the nonstoichiometric NiO lies in the peak widths, which are wider for the nonstoichiometric oxide. Crystallite sizes of the stoichiometric and nonstoichiometric NiO were calculated by two methods, (1) from the BET areas and NiO densities, assuming a shape factor of 5, and (2) by the Scherrer method, bearing in mind that particles larger than ~500 Å may not be detected by the Scherrer technique due to too little broadening. Table 6 shows the particle sizes obtained by both methods, which are always larger for the stoichiometric NiO. The particle sizes of the nonstoichiometric NiO are larger according to method (1) by a factor of 2; however, they are considerably larger, by a factor of 10, for the stoichiometric NiO, using the same method. In this respect, method (2) determines the mean crystal particle sizes irrespective of the degree of crystal conglomeration present, whereas method (1), because of the parameters used, is more sensitive to the conglomeration degree of the sample. Thus, stoichiometric NiO is far more conglomerated or sintered (particles about seven times larger) than the nonstoichiometric NiO.

X-Ray Photoelectron Spectroscopy

The binding energies (BE) of the Ni $2p_{3/2}$ peaks are summarized in Table 1. Catalysts 1, 2, and 3–5 obtained from hydrogen reduction of the stoichiometric NiO show BE values at 855.8–855.6 eV and 854.6–854.4 eV, corresponding to NiO and metallic Ni phases, respectively. However, the 0.2-eV shift toward lower BE in catalyst 2, when compared with catalyst 1, may be indicative of an incipient reduction of the stoichiometric NiO; this was not detected by XRD, probably because of the very small crystallite sizes present. Catalytic results of sample 2, with no metallic nickel phase detected by XRD (Table 1), also support the presence of incipiently reduced NiO, as it proves to be slightly active for the hydrogenation reaction tested.

For potassium-free nonstoichiometric NiO, catalysts 6–8 show the principal Ni $2p_{3/2}$ peak at BE ca. 855.8–855.6 eV. These values and the presence of a shake-up satellite slightly above 862 eV clearly indicate the presence of Ni^{2+} ions in the catalysts. However, catalysts 9–11 show BE values of Ni $2p_{3/2}$ in the region of 854.5–854.2 eV and complete disappearance of satellite structure, which confirms the presence of metallic Ni in the catalysts. Calculation of the ratio satellite-to-principal for the Ni $2p_{3/2}$ peaks for catalysts 6–8 also revealed that it was maximum for catalyst 6, slightly smaller for catalyst 7, and substantially smaller for catalyst 8. This fact together with the tendency of BE to decrease when passing from catalyst 6 to 8 can be taken as indicative of formation of incipient reduced nickel on the NiO surface, probably having such small particle sizes that the metallic nickel phase remains undetectable by XRD. These results are in complete agreement with those obtained from the temperature-programmed reductions, scanning electron microscopy, and catalytic activities, as shown before and below, respectively.

For potassium-doped catalysts we note the presence of NiO phases in catalysts 12, 13, and 17 and metallic nickel phases in catalysts 13 and 17, at 855.8 eV with presence of the typical NiO satellite, and around 854.4 eV, for catalysts 14–16, 18–21, with disappearance of satellite structure, respectively. The XPS technique also detects the reduction inhibiting effect of potassium upon the nonstoichiometric NiO when the BE values are compared at the same temperature of reduction. The BE values increase on increasing the potassium content, indicating a higher presence of the NiO phase. These results are in agreement with those from the XRD and TPR measurements. Finally, we should remark that even though the absolute values of the binding energies taken from the XPS literature show a spread of several eV, we should always consider, as a general valuable analysis, the relative behaviour of the nickel species in any particular spectra.

Field Emission-Scanning Electron Microscopy (FE-SEM)

The FE-SEM stereographic picture of catalyst 7 is shown in Fig. 5; this was taken in order to obtain better resolution and contrast at lower acceleration voltages. Catalyst 7 reduced at 463 K exhibits clear NiO octahedra, sometimes containing small aggregations of reduced nickel on their edges. In contrast, catalysts reduced at higher temperatures do not show clear NiO octahedra, but masses of reduced nickel (*26*). The backscattering image confirms, for catalyst 7, the different densities of both phases, which are higher for the aggregations and lower for the octahedra, as they correspond to metallic nickel and NiO, respectively.

Therefore, FE-SEM results confirm the presence of incipiently reduced nickel in the catalytically active catalysts prepared at reduction temperatures below 473 K, in complete agreement with the above results of XRD and XPS.

Catalytic Activity

Conversions and product distributions for the hydrogenation reaction of 1,6-hexanedi-

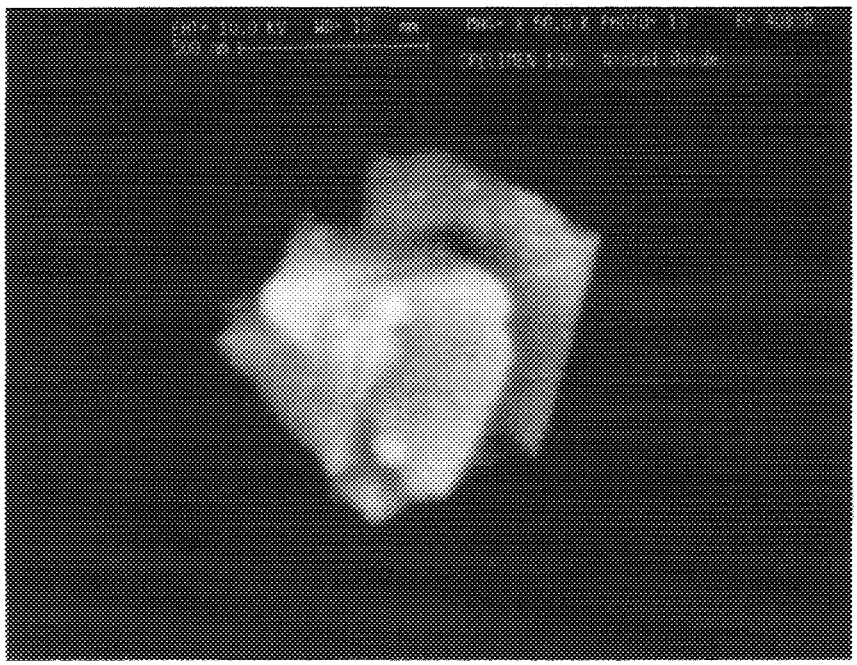

FIG. 5. Field emission-scanning electron micrograph taken from the surface of catalyst 7 (magnification ×50,000).

nitrile on catalysts 1–21, under the experimental conditions given before, are summarized in Table 1. Catalysts 1–5, obtained from the reduction of stoichiometric NiO, show increasing conversions with increased degree of reduction α. Conversion decreases for reduction temperatures higher than 623 K, where sintering starts to increase significantly. The observed conversions are always lower than those obtained from the reduction of nonstoichiometric NiO at the same degrees of reduction. This result agrees with that of the higher sintering observed for the starting stoichiometric NiO according to Table 6. Catalytic activities of catalysts 1–5 begin at temperatures about 100 K higher than those for catalysts 6–11, in agreement with the TPR results and activation energy data shown above, from which temperatures about 100 K higher are needed to start the reduction of the stoichiometric NiO, because of its higher activation energy, in comparison with the same parameters from the reduction of nonstoichiometric NiO. Selectivities of catalysts 1–5 toward 6-aminohexanenitrile are comparable to those obtained from catalysts 6–11, although at lower conversions, as mentioned.

The 1,6-hexanedinitrile conversion of catalysts 6–11 increases in parallel with the extent of reduction of the NiO phase up to 573 K, but it decreases at higher temperatures of NiO reduction. This can mainly be attributed to the surface area decrease because of sintering of the metallic nickel phase, which should cause a decrease of the surface active sites, especially those responsible for the production of azacycloheptane. Thus, 6-aminohexanenitrile can be 100% selectively obtained. Conversely, selectivities towards azacycloheptane follow the opposite trend; i.e., they are high or low for low or high 6-aminohexanenitrile selectivities, respectively, suggesting different active sites (*26*).

Conversions for the hydrogenation reac-

tion of adiponitrile on catalysts 12–21, under the experimental conditions given before, increase with parallel increase of reduction degrees, α, of the NiO phase, following a volcano profile for each potassium content. Maximum conversion values are obtained near the lower reduction temperature needed to reach 99.9% reduction. Conversions decrease at higher temperatures, probably due to a decrease of active area because of sintering of the metallic nickel phase, increasing selectivity towards 6-aminohexanenitrile. However, for higher potassium content as in catalysts 17–21, we observe 100% selectivity in 6-aminohexanenitrile at any conversion value. Thus, potassium seems to decrease the number of surface active sites, affecting the sites responsible for the production of azacycloheptane and 1,6-hexanediamine more than those of 6-aminohexanenitrile. Increasing potassium content decreases conversion at the same reduction temperature of potassium-doped NiO, because of the NiO-reduction-inhibiting character of potassium, in agreement with the TPR measurements and activation energy data shown before. Conversely, selectivities with respect to 1,6-hexanediamine and azacycloheptane also follow the opposite trend; i.e., they are high or low for low or high 6-aminohexane selectivity, respectively, suggesting different structural requirements for the active sites responsible for the production of 6-aminohexanenitrile with respect to those of 1,6-hexanediamine and azacycloheptane. Consequently, we may consider the adiponitrile hydrogenation for the selective production of primary amines as a structure-sensitive reaction.

Mechanism Proposal

From the above catalytic results we may conclude that selectivities towards 6-aminohexanenitrile are higher when the catalyst's potassium content is increased. The basicity increase, due to potassium, not only favours amine desorption, but also should modify the distribution of total available surface centres responsible for the different reaction products, as proposed.

Table 7 compiles the conversion and selectivity behaviour of the catalysts with respect to two external reaction parameters, reaction temperature and space velocity. We observe similar behaviour for the catalysts obtained from either the stoichiometric or the nonstoichiometric NiO, except for those which are potassium-doped. When 6-aminohexanenitrile is used as starting reactant a strong decrease of conversion for the potassium-doped catalysts is observed. The results obtained by varying either the external reaction parameters or the internal catalyst parameters show 6-aminohexanenitrile, 1,6-diaminohexane, and azacycloheptane as the only products of hydrogenation of 1,6-hexanedinitrile under the experimental conditions mentioned in this work. Neither secondary and tertiary amines nor dimeric products or imine intermediates were obtained in our process. According to Table 7, an increase of the space velocity causes an important increase of selectivity towards 6-aminohexanenitrile together with a small decrease of conversion. Also, a decrease of the reaction temperature increases the selectivity towards 6-aminohexanenitrile, in both cases using 1,6-hexanedinitrile as reactant. High space velocities and lower reaction temperatures (i.e., high 6-aminohexanenitrile selectivities) should prevent the aminoimine intermediate of Scheme 1 from forming, presumably because of the easier 6-aminohexanenitrile desorption from the surface (at high space velocities) and the different activation energy barriers needed for the production of azacycloheptane and 1,6-diaminohexane, respectively. Consequently, different nickel surface centres should be responsible for the selective hydrogenation of 1,6-hexanedinitrile to 6-aminohexanenitrile, azacycloheptane, and 1,6-diaminohexane, respectively. Sintering of undoped nickel smooths its surface, cancelling the centres responsible for the hydrogenation of the aminoimine intermediate that yield azacycloheptane or 1,6-diamino-

TABLE 7

Catalytic Behavior of Nickel Catalysts vs External Reaction Parameters

Catalyst	Space velocity (h^{-1})	Reaction temp. (K)	Conversion (%)	Selectivity (%)[a]		
				Monoamine	Diamine	Others
9	1500	443	100	0	30	70
9	750	443	100	0	10	90
9	3000	443	80	70	15	15
9	1500	463	100	0	15	85
9	1500	423	90	50	30	20
9[b]	1500	443	100	—	20	80
19	1500	443	50	100	0	0
19	1500	423	40	100	0	0
19	1500	463	70	80	5	15
19	750	443	65	90	0	10
19[b]	1500	443	20	—	25	75

[a] Monoamine = 6-aminohexanenitrile; diamine = 1,6-hexanediamine; others = azacycloheptane, mainly. Reaction conditions: 1,6-hexanedinitrile hydrogenation at 443 K, 1 atm pressure, and space velocity 1500 h^{-1}.
[b] 6-aminohexanenitrile hydrogenation under the same reaction conditions.

hexane. Similarly, increasing potassium loading cancels the more acidic centres, i.e., the coordinatively more unsaturated nickel atoms on the external surface, decreasing conversion, but increasing selectivity towards 6-aminohexanenitrile. Azacycloheptane and 1,6-diaminohexane are formed generally together, because of their original common intermediate. Consequently, the reaction paths, under the reaction conditions used and in agreement with the proposed mechanism, may be oriented as follows: (a) a path towards 6-aminohexanenitrile is favoured by sintered undoped nickel or potassium-doped nickel, as in catalysts 17–21; (b) the molar ratio production of azacycloheptane/1,6-diaminohexane increases for very active unsintered potassium-free nickel catalysts, especially when low space velocities and high reaction temperatures are used; (c) the molar ratio production of azacycloheptane/1,6-diaminohexane decreases for very active unsintered nickel catalysts, if high space velocities and low reaction temperatures are used.

CONCLUSIONS

The activation energies of reduction of stoichiometric and nonstoichiometric potassium-free and potassium-doped NiO were calculated from the TPR data, using two compared theoretical methods. Nonstoichiometric NiO shows the lower initial activation energy of reduction, converging the calculated values for all NiO forms when reduction is complete, for a zero reaction order. Doping potassium inhibits NiO reduction, and highly sintered NiO with low BET area, as in stoichiometric NiO, shows a higher initial activation energy for starting the autocatalytic nucleation.

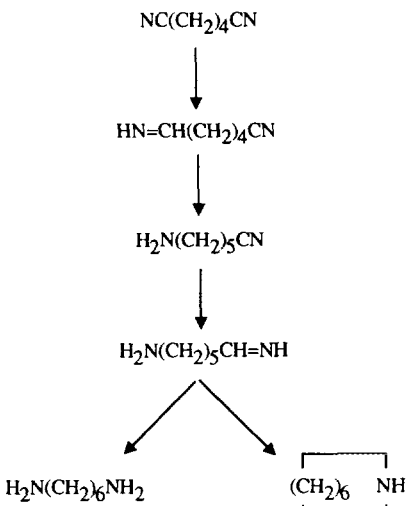

SCHEME 1

Studies of the chemical preparation, BET surface areas, XRD, XPS, SEM, and activities of the catalysts were also carried out for their structural characterizations vs the catalytic hydrogenation of 1,6-hexanedinitrile. Surface areas decrease when NiO reduction temperature increases, being also generally lower for stoichiometric NiO. Larger crystallite sizes for stoichiometric unreduced NiO are calculated. Only high selectivities to 6-aminohexanenitrile at very low conversions are observed for catalysts coming from the stoichiometric NiO precursors.

XRD, XPS, TPR, and FE-SEM measurements detect incipiently reduced nonstoichiometric NiO at 463–498 K. Nonstoichiometric NiO precursors become completely reduced at temperatures close to 500 K, but the resulting Ni phase is not well suited for the selective production of 6-aminohexanenitrile. Reduction temperatures as high as 623–673 K are required to obtain catalysts selective towards 6-aminohexanenitrile. On the other hand, doping with potassium inhibits reduction of NiO precursors, requiring temperatures as high as 573–623 K to reach complete reduction. Potassium concentrations of 10.5×10^{-4} g K_2O/g Ni cause a drastic increase of selectivity in 6-aminohexanenitrile for catalysts reduced at any temperature between 473 and 723 K. Consequently, catalysts 17–21 are suitable for the manufacture of 6-aminohexanenitrile, with 100% selectivities and conversions in the range 50%–60% and higher, from the catalytic hydrogenation of 1,6-hexanedinitrile, having potential interest for the manufacture of nylon-6,6 on an industrial scale. A mechanism is proposed where the reaction paths are oriented not only by the external reaction parameters but also by the surface structures and the doping potassium contents of the nickel catalysts.

ACKNOWLEDGMENT

We gratefully acknowledge the support of this work by the Comisión Interministerial de Ciencia y Tecnología (Project PB89-0240).

REFERENCES

1. Greenfield, H., *Ind. Eng. Chem. Prod. Res. Dev.* **6,** 142 (1967).
2. Pasec, J., Kostova, N., and Dvorak, B. *Collect. Czech. Chem. Commun.* **46,** 1011 (1981).
3. Bolle, J., French Patent 2 063 378 (1971).
4. Hioki, K., Hirokawa, K., Kuka, Y., and Shimade, A., *Jpn. Kokai Tokkyo Koho* 75 47 909 (1975).
5. Frank, G., and Neubauer, G. BASF AG., German Patent 3 402734 A1 (1984).
6. Jerzykiewicz, W., Krasnodebski, Z., and Bekierz, G., Polish Patent 115 999 (1983).
7. Kuthens, C. E., and Lanier, L. M., U.S. Patent 4 429 159 (1984).
8. Taira, S., Japanese Patent 70 32 410 (1970).
9. Toyo Rayon Co., French Patent 1 530 809 (1968).
10. Diffenback, R. A., French Patent 2 149 987 (1973).
11. Taira, S., Japanese Patent 69 05 844 (1969).
12. Alain, R. J., U.S. Patent 4 375 003 (1976).
13. Uehara, R., Horii, T., Imai, T., Tomita, Y., and Yamano, K., *Jpn. Kokai Tokkyo Koho* 76 78 795 (1976).
14. Societé des Usines Chimiques Rhône Poulenc, French Patent 2 248 265 (1975).
15. Kuroda, A., and Taira, S., Japanese Patent 72 31 833 (1972).
16. Mares, F., Galle, J. E., Diamond, S. E., and Regina, F. J., *J. Catal.* **112,** 145 (1988).
17. Adam, K., and Haarer, E., BASF, A. G., French Patent 1 483 300 (1967).
18. Augustine, R. L., *Catal. Rev.* **13,** 285 (1976).
19. Fierro, J. L. G., Medina, F., Salagre, P., and Sueiras, J. E., *J. Mol. Catal.* **61,** 197 (1990).
20. Medina, F., Salagre, P., Fierro, J. L. G., and Sueiras, J. E., *J. Mol. Catal.* **68,** L17 (1991).
21. Robertson, S. D., McNicol, B. D., De Baas, J. H., Kloet, S. C., and Jenkins, J.W., *J. Catal.* **37,** 424 (1975).
22. Hurst, N. W., Gentry, S. J., Jones, A., and McNicol, B. D., *Catal. Rev. Sci. Eng.* **24,** 233 (1982).
23. Coats, N. W., and Redfern, J. P., *Nature* **201,** 68 (1964).
24. Ozawa, T., Flynn, J. H., and Wall, L. A., *J. Therm. Anal.* **2,** 301 (1970).
25. Zabala, J. M., Grange, P., and Delmon, B., *C.R. Seances Acad. Sci.* **561,** 279 (1974).
26. Medina, F., Salagre, P., Fierro, J. L. G., and Sueiras, J. E., *in* "XIII Simposio Iberoamericano de Catálisis Consejo Superior de Investigaciones Científicas (Ed.), Segovia, 6–10 July, 1992" p. 327.
27. Medina, F., Salagre, P., Fierro, J. L. G., and Sueiras, J. E., *J. Mol. Catal.*, **81**(3), 363 (1993).
28. Medina, F., Salagre, P., Fierro, J. L. G., and Sueiras, J. E., *Appl. Catal.*, **92,** 131 (1992).
29. Medina, F., Salagre, P., Fierro, J. L. G., and Sueiras, J. E., *J. Mol. Catal.*, **81**(3), 387 (1993).